Article

Journal of Nanoscience and Nanotechnology
Vol. 14, 7307–7314, 2014
www.aspbs.com/jnn

The UV/Fenton Degradation of Tetrabromobisphenol A Catalyzed by Nanocrystalline Chromium Substituted Magnetite

Yuanhong Zhong[1,3], Xiaoliang Liang[1], Zisen He[1,3], Wei Tan[1,3], Hongping He[1,*], Runliang Zhu[1], Yin Zhong[2], Jianxi Zhu[1], Peng Yuan[1], and Zheng Jiang[4]

[1] *Key Laboratory of Mineralogy and Metallogeny, Guangzhou Institute of Geochemistry, Chinese Academy of Sciences, 511 Kehua Street, Guangzhou 510640, China*
[2] *Pearl River Delta Research Center of Environment Pollution and Control, Guangzhou Institute of Geochemistry, Chinese Academy of Sciences, Guangzhou 510640, China*
[3] *University of Chinese Academy of Sciences, Beijing 100049, China*
[4] *SSRF, Shanghai Institute of Applied Physics, Chinese Academy of Sciences, Shanghai 201800, China*

The heterogeneous UV/Fenton degradation of tetrabromobisphenol A (TBBPA) catalyzed by nanocrystalline Fe_3O_4 and $Fe_{2.04}Cr_{0.96}O_4$ was investigated, with focus on the influence of UV light and initial pH, degradation pathways and effect of Cr substation. The catalysts were prepared by a precipitation-oxidation method and characterized by chemical analysis, XRD, XAFS, TG-DSC, BET surface area and magnetometer. At pH 6.7 and under UV irradiation, almost complete degradation of TBBPA by $Fe_{2.04}Cr_{0.96}O_4$ was accomplished within 240 min, and the leaching Fe ions were negligible. The substitution of chromium greatly increased the BET specific surface area and surface hydroxyl amount, which improved the heterogeneous UV/Fenton catalytic activity of magnetite. Moreover, Cr^{3+} on the octahedral sites enhanced the electron transfer process in the magnetite structure to accelerate the $^{\bullet}OH$ generation. The produced $^{\bullet}OH$ radicals preferentially attacked the C—Br bonds of TBBPA and then β-cleavaged the C—C bonds between benzene rings and isopropyl groups. The above results are of great significance for well understanding the effect of transition metal substitution on the UV/Fenton catalytic activity of magnetite and prospecting the application of magnetite minerals in environmental purification.

Keywords: Magnetite, Isomorphous Substitution, Catalytic Activity, UV/Fenton, Tetrabromobisphenol A.

1. INTRODUCTION

During the last decade, growing interest has been evoked in the application of iron oxides in industry and environmental processes,[1–6] especially for the transition metal substituted magnetites as catalysts with nano-size.[7–14] One of the most promising applications should be as heterogeneous Fenton catalysts in the degradation of organic pollutants, e.g., dyes, phenol and hydroquinone,[15–18] due to the merits of easy handling, low cost, nontoxicity and environmental harmony.[19–22] It has been widely acknowledged that the catalytic activity of magnetite is greatly dependent on the species, valence and occupancy of substituting metals. Costa et al. indicated the remarkable effect of Co and Mn substitution on enhancing the reactivity of magnetite towards H_2O_2 decomposition and methylene blue degradation while Ni showed an inhibitive effect.[21] Recently, the Fenton catalytic activity of Cr substituted magnetite also has been investigated in the degradation of aqueous cationic and anionic dyes.[23] It has been proved that the improvement extent varied with the substitution level and the degradation mechanism was related to dye species. In addition, the photo-catalysis of UV/Fenton process by substituted magnetites also has attracted great attention, because the introduction of ultraviolet light into Fenton system obviously accelerates the pollutant degradation and mineralization.[24] For instance, Ti^{4+} substitution

*Author to whom correspondence should be addressed.

in magnetite greatly improved the UV/Fenton degradation of tetrabromobisphenol A (TBBPA) under neutral pH condition, and the degradation efficiency increased with the increment of titanium content.[25] TBBPA is a widely used brominated flame retardant, one of persistent organic pollutants (POPs) with negative effect on various aspects of mammalian and human physiology.[26–29] However, to the best of our knowledge, the application of other substituted magnetites in the UV/Fenton degradation of TBBPA has been still quite limited, especially in terms of the process conditions, degradation pathways and mechanism.

In this study, the catalytic activity of nanocrystalline Cr substituted magnetite ($Fe_{3-x}Cr_xO_4$) has been investigated in the heterogeneous UV/Fenton degradation of TBBPA. Effect of initial pH and UV irradiation, degradation pathways and reaction mechanism were discussed in detail. The obtained results are of high importance for well understanding the role of substitution on the catalytic activity of magnetite towards UV/Fenton reaction and developing novel and efficient catalysts for POPs degradation.

2. MATERIALS AND METHODS

2.1. Magnetite Synthesis and Characterization

All the chemicals and reagents used in this study were of analytical grade and used as received. The magnetite samples Fe_3O_4 and $Fe_{2.04}Cr_{0.96}O_4$ was synthesized by a precipitation-oxidation method as described in literatures.[25, 30] From previous researches, all the magnetite samples prepared by this method were in the nanosize range of 20 to 100 nm.[13, 24] The chemical analysis results showed that the molar ratio between Fe and Cr in $Fe_{2.04}Cr_{0.96}O_4$ was about 2:1.

Powder X-ray diffraction (PXRD) patterns were recorded between 10° and 80° (2θ) at a step of 1° min^{-1} on a Bruker D8 advance diffractometer with Cu Kα radiation (40 kV and 40 mA). BET specific surface area was measured on the basis of N_2 physisorption capacity at 77 K on an ASAP 2020 instrument, after degassed at 433 K for 12 h. X-ray absorption fine structure (XAFS) spectrum of $Fe_{2.04}Cr_{0.96}O_4$ was obtained on the new Wiggler beamline BL14W1 of Shanghai Synchrotron Radiation Facility (SSRF). The storage ring was operated at 3.5 GeV electron energy and 150–300 mA beam current. The BL14W1 was a focused X-ray beamline, using a Si (111) double crystal monochromator. The Cr *K*-edge absorption spectrum was recorded in the transmission mode. Data analyses were performed using IFEFFIT software package. Thermogravimetric and differential scaning calorimetry (TG-DSC) analyses were synchronously performed on a Netzsch STA 409 PC instrument. Approximately 10 mg of finely ground sample was heated in a corundum crucible with heating rate 10 °C min^{-1} under N_2 atmosphere. Point of zero charge (pH_{pzc}) was determined by acid-base potentiometric titration.[31] Isothermal remanent magnetization (*IRM*) and anhysteretic remanent magnetization (*ARM*) were measured on a JR6A spinner magnetometer. The leaching Fe ion concentration was analyzed on a PE-3100 flame atomic absorption spectrophotometer (FAAS).

2.2. TBBPA Degradation

TBBPA degradation experiment was carried out in a home-made photo-reactor with or without UV light source. Methanol was chosen as the hydrotropic agent to increase the solubility of TBBPA, and the volume ratio of methanol to water was optimized at 2:3 in the preliminary experiment. The volume of TBBPA solution was 500 mL. The dosage of catalyst was 0.5 g L^{-1} while the initial concentrations of TBBPA and H_2O_2 were 20 mg L^{-1} and 10 mmol L^{-1}, respectively. The initial pH of solution was adjusted by HCl (0.1 mol L^{-1}) and NaOH (0.1 mol L^{-1}) solution. Before the TBBPA degradation experiment, the suspension containing catalyst and TBBPA was firstly stirred for 60 min in dark to achieve adsorption equilibrium. Then 5.0 mL of suspension was filtered through a 0.22 μm nylon filter to separate the magnetite, and the equilibrium solution was sampled for TBBPA concentration analysis. The degradation was initiated by simultaneously adding H_2O_2 and exposing to natural light or UV light ($\lambda = 365$ nm). At given intervals, the reaction solution was sampled and filtered for TBBPA concentration analysis.

The TBBPA concentration was analyzed on a Shimadzu LC-20A high performance liquid chromatography (HPLC), equipped with an Inertisil ODS-SP column (150 mm × 4.6 mm, 5 μm particles). The mobile phase was a mixture of methanol and 0.2% glacial-acetic-acid solution at a volumetric ratio of 4:1. The degradation products of TBBPA were analyzed on a gas chromatographic mass spectrometry (GC-MS), equipped with a Rxi-5ms fused silica capillary column (DB-5MS, 30 m × 0.25 mm × 0.25 μm).

3. RESULTS AND DISCUSSION

3.1. Magnetite Samples Characterization

The PXRD patterns (Fig. 1) of magnetite samples well correspond to the standard card of magnetite (JCPDS: 19-0629), indicating that the synthetic samples have well crystallized spinel structure. The lattice parameters (a_0) for Fe_3O_4 and $Fe_{2.04}Cr_{0.96}O_4$ (Table I) are 0.8392 and 0.8403 nm, and the average crystal sizes are 25.9 and 25.4 nm, which shows that the prepared samples are nanocrystalline magnetites. Cr substitution does not obviously impact on the crystal structure of magnetite.

XAFS characterization was carried out to probe the valence and occupancy of chromium in the substituted magnetite samples. The detailed discussion for X-ray absorption near-edge spectrum (XANSE) of $Fe_{2.04}Cr_{0.96}O_4$ has been presented elsewhere.[32] The Cr atoms in $Fe_{2.04}Cr_{0.96}O_4$ are in valence of +3 and occupy the octahedral sites. Herein, extended X-ray absorption fine structure

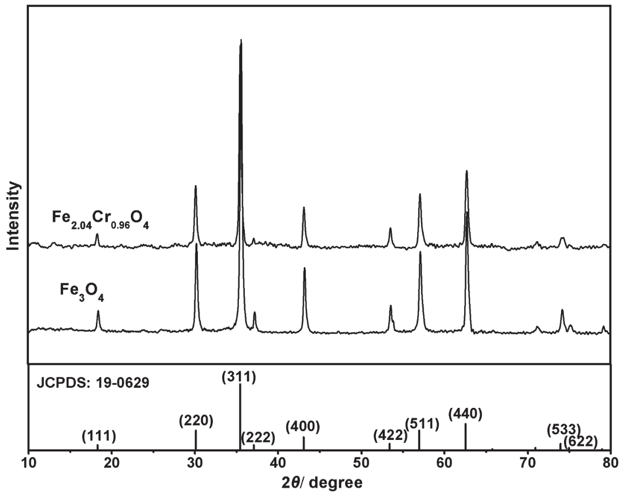

Figure 1. X-ray diffraction patterns of Fe_3O_4 and $Fe_{2.04}Cr_{0.96}O_4$.

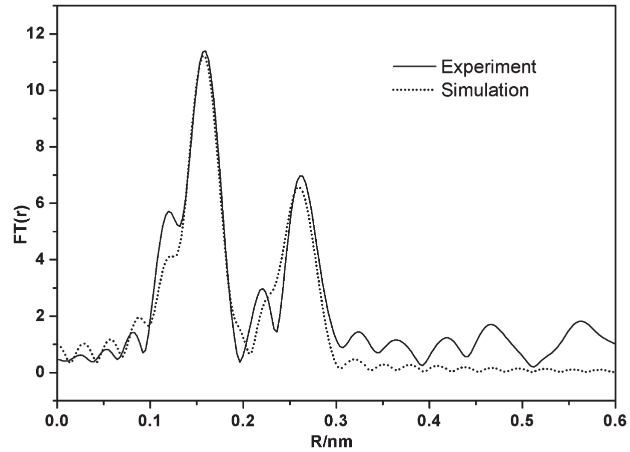

Figure 2. Fourier transform curve (full line) from the Cr *K*-edge EXAFS spectrum of $Fe_{2.04}Cr_{0.96}O_4$ and the best fitting spectrum (dashed line).

(EXAFS) analysis was performed to determine the local atomic structure of Cr in $Fe_{2.04}Cr_{0.96}O_4$. Figure 2 shows the Fourier Transform (FT) curve and the best fitting characteristic of $Fe_{2.04}Cr_{0.96}O_4$. On the FT curve, the first peak is ascribed to the first-nearest Cr–O shell while the second one is ascribed to the first-nearest Cr–Cr shell.[33] From the fitted crystal structure of $Fe_{2.04}Cr_{0.96}O_4$, Cr atom is coordinated with six nearest oxygen atoms and the Cr–O distance is 2.055 Å (Table II). The fitting curve well corresponds to the obtained curve of $Fe_{2.04}Cr_{0.96}O_4$, indicating that the Cr atoms in $Fe_{2.04}Cr_{0.96}O_4$ are in the center of octahedrons.

As shown in Figure 3 and Table I, the BET specific surface area of $Fe_{2.04}Cr_{0.96}O_4$ (110.0 m^2 g^{-1}) is about six times larger than that of Fe_3O_4 (18.9 m^2 g^{-1}). The isomorphous substitution of chromium obviously increases the specific surface area of magnetite.

The surface hydroxyl (M–OH) are the functional groups on iron oxide surface and have vital influence on surface properties, e.g., surface acidity (Brønsted acid and Lewis acid), adsorption[34] and photocatalysis.[35] The amount of surface hydroxyl in two magnetite samples was determined by TG-DSC analysis (Table I).[23] The surface hydroxyl amount of $Fe_{2.04}Cr_{0.96}O_4$ (6.60%) is much higher than that of Fe_3O_4 (0.48%), demonstrating that Cr substitution greatly increases the surface hydroxyl amount.

Table I. The characterization results of Fe_3O_4 and $Fe_{2.04}Cr_{0.96}O_4$.

Parameters	Fe_3O_4	$Fe_{2.04}Cr_{0.96}O_4$
Lattice parameter, a_0/nm	0.8392	0.8403
Average crystal size/nm	25.9	25.4
BET specific surface/m^2 g^{-1}	18.9	110.2
Surface hydroxyl amount/%	0.48	6.60
pH^a_{pzc}	6.96	6.85
SIRM[b]/emu g^{-1}	15.7	6.1
ARM[b]/A m^{-1}	0.044	0.070
Hc/mT	−32.3	−23.7

Notes: [a]pH_{pzc}: point of zero charge; [b]room temperature.

The magnetic properties of two magnetite samples were induced by the alternating field to investigate the stepwise *IRM* acquisition and the demagnetization curve at room temperature. The obtained results show that both the nanocrystalline magnetites are magnetic materials (Fig. 4 and Table I), which are benefit for their recycle in future application. Compared to Fe_3O_4, the *SIRM* decreases about 61% after Cr substitution. The *SIRM* value of $Fe_{2.04}Cr_{0.96}O_4$ is 6.1 emu g^{-1} at 1000 mT while that of Fe_3O_4 is 15.7 emu g^{-1}. $Fe_{2.04}Cr_{0.96}O_4$ with lower *SIRM* possesses the higher *ARM*. These observed variations in magnetic parameters might be ascribed to the substitution of Cr^{3+} for Fe^{3+} in magnetite structure and the decrease in grain size by Cr substitution.[36]

3.2. TBBPA Degradation

3.2.1. Effect of UV Radiation

The degradation processes of TBBPA through heterogeneous Fenton reaction catalyzed by $Fe_{2.04}Cr_{0.96}O_4$ at near neutral pH were investigated with or without UV-light source (Fig. 5). Only about 4% of TBBPA was removed under natural light. For the system with UV radiation in wavelength of 365 nm, the TBBPA removal was rather efficient. 20 mg L^{-1} of TBBPA was almost degraded after 240 min reaction.

In the Fenton degradation without UV radiation, $^{\bullet}OH$ radical was produced by the reaction between $\equiv Fe^{II}$ on magnetite surface and H_2O_2 through the Haber-Weiss mechanism (Eq. (1)). But it was obvious that the amount

Table II. Fitting parameters of Cr^{3+} EXAFS in magnetite.

Shell	N^a	R^b (Å)	σ^2 (Å^2)^c
Cr–O	6	2.055 (0.011)	0.002
Cr–Cr	6	2.961 (0.026)	0.008

Notes: [a]*N*: the number of backscattering atoms around the absorbing Cr atom; [b]*R*: the absorber-backscatterer distance; [c]σ^2: the Debye-Waller value.

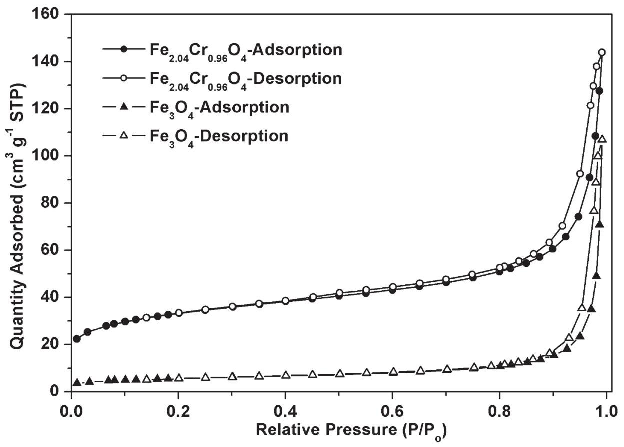

Figure 3. Nitrogen adsorption–desorption curves of Fe_3O_4 and $Fe_{2.04}Cr_{0.96}O_4$.

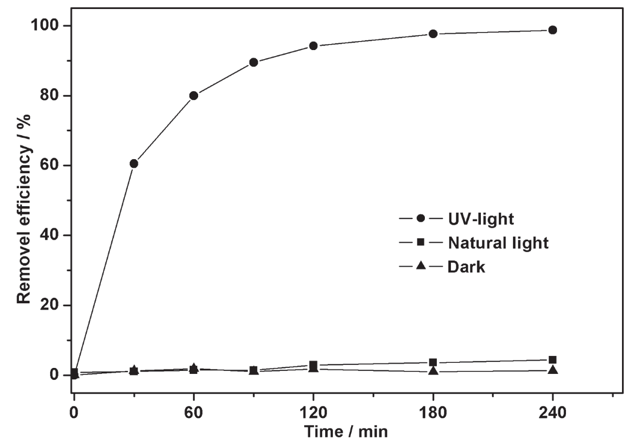

Figure 5. Effect of UV light on TBBPA degradation.

of produced $^{\bullet}OH$ radicals was not enough for complete degradation of TBBPA. But the introduction of UV irradiation greatly accelerated the degradation of TBBPA. From previous research, the vital role of UV light in UV/Fenton reaction may originate from two aspects. The $^{\bullet}OH$ radicals were generated by photolysis of H_2O_2 (Eq. (2)).[37] $^{\bullet}OH$ radical was the most active oxidant with a quite high redox potential and could destroy the TBBPA molecule. Moreover, under UV radiation $\equiv Fe^{III}$ could be effectively reduced to $\equiv Fe^{II}$ with stronger catalytic activity for Fenton reaction (Eq. (3)).

$$\equiv Fe^{II} + H_2O_2 \rightarrow \equiv Fe^{III} + {}^{\bullet}OH + {}^{\bullet}OH^- \quad (1)$$

$$H_2O_2 + h\nu \rightarrow 2\,{}^{\bullet}OH \quad (2)$$

$$\equiv Fe^{III} + H_2O_2 + h\nu \rightarrow \equiv Fe^{II} + 2\,{}^{\bullet}OH \quad (3)$$

3.2.2. Effect of pH

TBBPA is an ionizable hydrophobic organic compound and its ionized constant pKa was 7.5 for pKa_1 and 8.5 for pKa_2.[38] The aqueous solubility and degradation efficiency of TBBPA should be pH dependent. The effect of pH on the TBBPA adsorption and degradation by $Fe_{2.04}Cr_{0.96}O_4$ was investigated at different initial pH (Fig. 6). Obviously, the adsorption efficiency was strongly dependent on the initial pH. TBBPA was hardly adsorbed on the $Fe_{2.04}Cr_{0.96}O_4$ surface at pH above 7.7, but the adsorption efficiency gradually increased with the decrease of pH under 7.7. The adsorption was more favorable in acid condition. In the tested pH range, TBBPA existed as molecule and anion. When the initial pH was below the pKa_1 of TBBPA ($pKa_1 = 7.5$), TBBPA was adsorbed onto the magnetite surface in form of molecular. But when the solution pH was above pKa_1 of TBBPA, TBBPA was mainly anionic and the magnetite surface was negatively charged. The electrostatic repulsion between TBBPA and magnetite surface was dominant, resulting in the decrease of TBBPA adsorption. Similar effect of initial pH was previously reported in TBBPA adsorption on soil.[39]

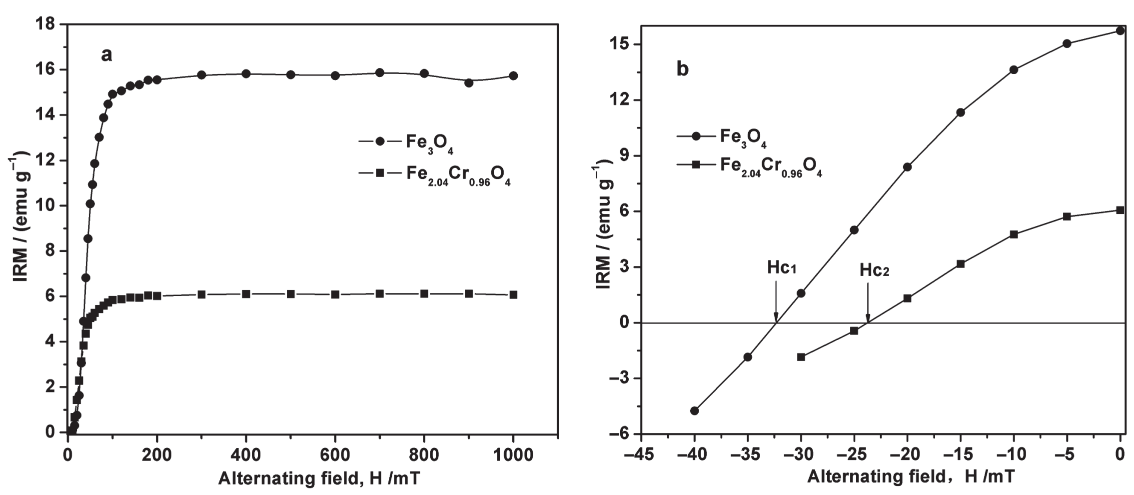

Figure 4. The magnetization curves of Fe_3O_4 and $Fe_{2.04}Cr_{0.96}O_4$ at room temperature. ((a) The stepwise *IRM* acquisition until achieving saturation; (b) The alternating field demagnetization curves for determination of remanent coercivity).

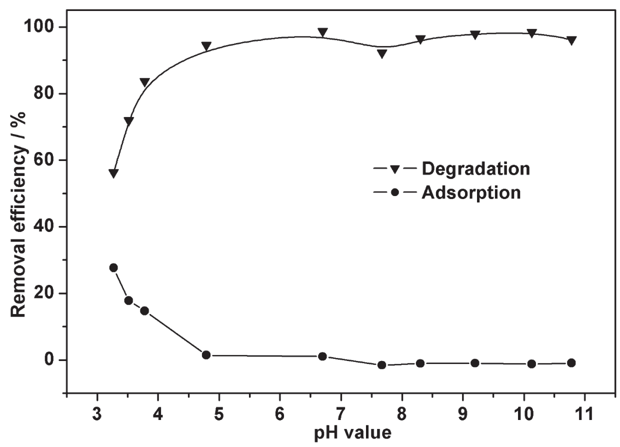

Figure 6. Effect of intial pH on TBBPA adsorption and degradation by $Fe_{2.04}Cr_{0.96}O_4$.

But for TBBPA degradation, the pH effect was completely different (Fig. 6). The removal efficiency was about 56% at the pH of 3.2. With the pH increase from 3.2 to 6.7, close to the pH_{pzc} of $Fe_{2.04}Cr_{0.96}O_4$ ($pH_{pzc} = 6.85$), the TBBPA removal efficiency gradually increased. However, in the pH range of 6.7 to 10.8, the TBBPA removal did not increase obviously. The results suggested that the degradation efficiency of TBBPA were dependent to the pH_{pzc} of magnetite rather than the *pK*a of TBBPA.

The effect of pH on degradation kinetics of TBBPA were also investigated (Fig. 7). All the degradation processes were well fitted by the pseudo-first-order rate equation (Eq. (4)) with correlation coefficients higher than 0.93.

$$-\ln(C_t/C_0) = k_{app}t \qquad (4)$$

where C_0 and C_t are the TBBPA concentrations at the initial time and different reaction time t, mg L^{-1}. k_{app} is the apparent pseudo-first-order rate constant, min^{-1}.

Table III. The kinetic parameters of TBBPA UV/Fenton degradation in different pH solution.

pH	$10^2 k_{app}/min^{-1}$	$t_{1/2}/min$	R^2
10.8	1.37	42.9	0.993
10.0	1.19	56.4	0.993
9.2	1.59	37.0	0.986
8.3	1.44	43.6	0.986
7.7	1.08	53.6	0.983
6.7	1.79	16.1	0.962
4.8	1.19	32.8	0.951
3.8	0.68	57.5	0.948
3.5	0.46	84.2	0.931
3.2	0.20	176.6	0.982

Table III shows the rate constant k_{app} and half-life $t_{1/2}$ for TBBPA degradation in Figure 7. Among these processes, the maximum degradation efficiency of TBBPA catalyzed by $Fe_{2.04}Cr_{0.96}O_4$ was obtained at initial pH 6.7, with the highest k_{app} (0.0179 min^{-1}) and 16.1 min needed for 50% TBBPA removal. The k_{app} slightly decreased along with the initial pH increased to the alkaline range, and significantly decreased when the initial pH decreased to 3.2. At initial pH 3.2, the $t_{1/2}$ for TBBPA degradation was about 176.6 min, over 10 times more than that at pH 6.7. The comparative study between adsorption and degradation showed that higher adsorption capacity did not result in higher degradation efficiency, suggesting that the role of magnetite in UV/Fenton degradation was mainly to decompose H_2O_2 for $^{\bullet}OH$ radical generation but not to adsorb TBBPA for degradation.

The initial pH not only influenced the photo-catalytic performance of catalysts, but also affected the Fe leaching from catalyst surface.[40] From previous research, when the solution pH was below 4.0, the iron dissolution became obvious and the degradation would be homogeneous process.[41] Thus, to optimize the initial pH for

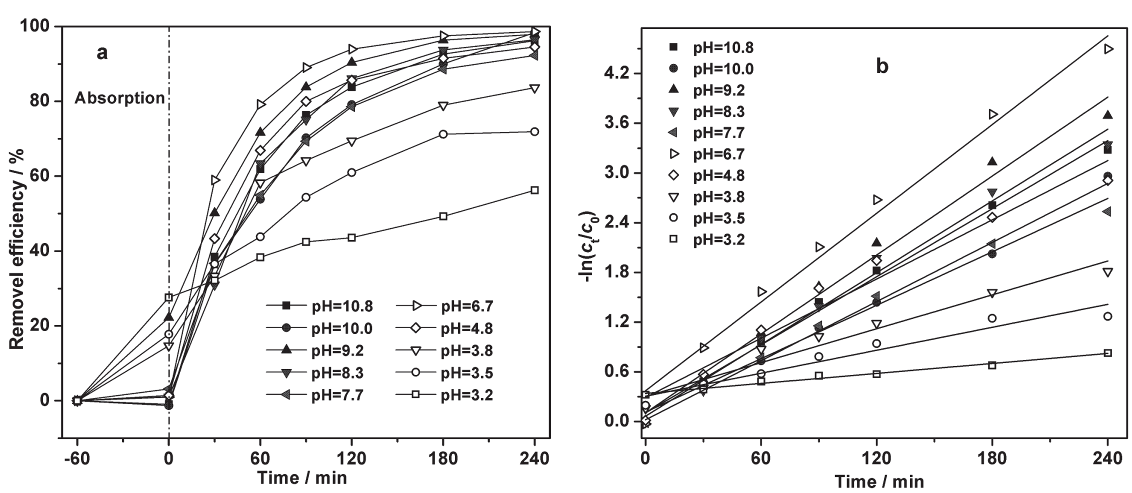

Figure 7. Kinetic process of TBBPA degradation through UV/Fenton reaction catalyzed by $Fe_{2.04}Cr_{0.96}O_4$ (a) and fitted by pseudo-first-order equation (b) (TBBPA: 20 mg L^{-1}, H_2O_2: 10 mmol L^{-1}, catalyst dosage: 0.50 g L^{-1}; 500 mL, 25 °C).

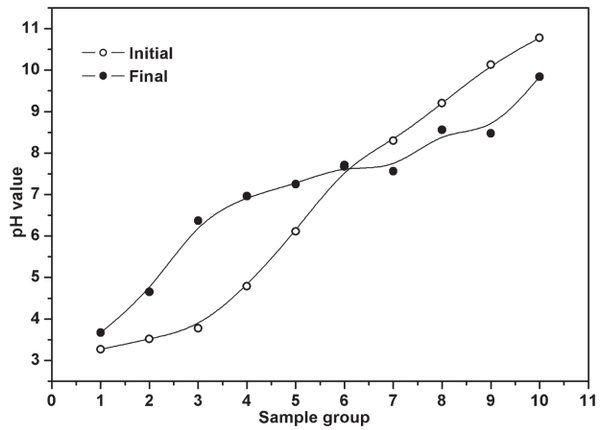

Figure 8. The pH variety before and after UV/Fenton reaction catalyzed by $Fe_{2.04}Cr_{0.96}O_4$.

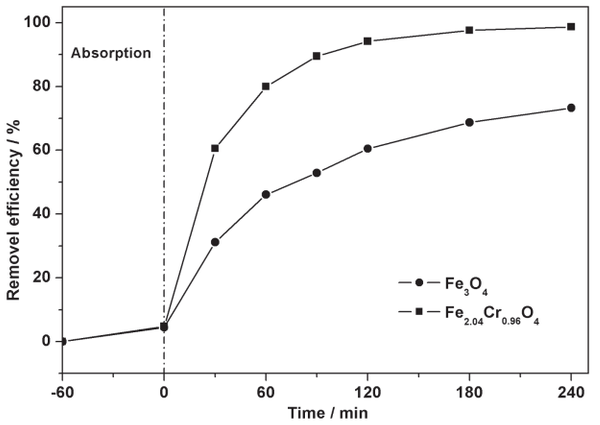

Figure 9. Comparison in the TBBPA degradation efficiency through UV/Fenton reaction between Fe_3O_4 and $Fe_{2.04}Cr_{0.96}O_4$. (TBBPA: 20 mg L^{-1}, H_2O_2: 10 mmol L^{-1}, catalyst dosage: 0.50 g L^{-1}; 500 mL, pH: 6.5, 25 °C).

maximum removal efficiency of TBBPA, it was necessary to simultaneously track the pH variety during degradation to avoid the Fe leaching. As shown in Figure 8, when the initial pH varied from 3.2 to 7.7, all the final pH after 240 min reaction increased to the value close to the pH_{pzc} of $Fe_{2.04}Cr_{0.96}O_4$, ascribed to the buffering effect of hydroxyl groups on magnetite surface. But for the systems with initial pH higher than 7.7, the final pH decreased but was still higher than 6.0, which was ascribed to the appearance of several medium acidic products during TBBPA degradation. Based on the degradation efficiency, pH variety and further application potential, the optimum initial pH should be neutral. The concentration of leaching iron in the system with initial pH 6.7 was also tracked to see the reusability of $Fe_{2.04}Cr_{0.96}O_4$. All the dissolved iron concentrations during the degradation were below detection limit (DL) of FAAS, indicating that TBBPA degradation by $Fe_{2.04}Cr_{0.96}O_4$ at initial pH 6.7 was the heterogeneous process.

3.3. Improvement Mechanism of Cr Substitution

From previous researches, Fenton and UV/Fenton catalytic activity of magnetite were improved by Cr^{3+} [23] and Ti^{4+} substitution,[25] and the improvement extent depended on the substitution level. Additionally, with larger specific surface area and more surface hydroxyl amount, magnetite exhibited better catalytic performance in organic pollutant degradation. As seen in Figure 9, the presence of Cr^{3+} in magnetite structure obviously improved the UV/Fenton catalytic activity of magnetite in TBBPA degradation. It should be related to the increased specific surface area and surface hydroxyl amount of magnetite by Cr substitution (Table I).[23, 25] With the increase of specific surface area of magnetite, the contact frequency between magnetite surface and reactant molecules was enhanced,[42] which increased the reaction rate. Moreover, the superficial hydroxyl groups on magnetite surface directly accepted photo-generated holes under UV irradiation.[43, 44] and adsorbed H_2O_2 to produce $^{\bullet}OH$ radicals.[45, 46]

Besides, the catalytic activity of magnetite was mainly dependent on the octahedral cations in spinel structure, as the octahedral sites were almost exclusively exposed at the surface of the spinel structure.[16] As Cr^{3+} almost occupied the octahedral site, it improved the electron transfer between Cr^{3+} and Fe^{2+}, and the reduced Cr^{2+} could participate in the heterogeneous Fenton reaction on the thermodynamic view (Eq. (5)). It should be another reason for the improvement of UV/Fenton catalytic activity of magnetite by Cr substitution.

$$\equiv Cr^{II} + H_2O_2 \rightarrow \equiv Cr^{III} + {}^{\bullet}OH + {}^{\bullet}OH^{-}, \quad \Delta E = 2.184\ V \tag{5}$$

Additionally, the reused $Fe_{2.04}Cr_{0.96}O_4$ still retained its catalytic activity after three cycles (data not showed). Based on the stronger activity and good reusability of $Fe_{2.04}Cr_{0.96}O_4$, it should be a promising catalyst for TBBPA degradation.

3.4. Degradation Pathways

To further investigate the catalytic activity of Fe_3O_4 and $Fe_{2.04}Cr_{0.96}O_4$ in heterogeneous UV/Fenton degradation of TBBPA, the degradation products in their existing systems were identified by GC-MS. The concentrations of detected degradation products were determined by comparing their relative peak area to that of TBBPA. In the system containing Fe_3O_4, eight intermediate products were found after 240 min degradation. About 40% (relative percentage composition) of the detected compounds was TBBPA and approximate 45% were tribromobisphenol A (TriBBPA, Product **1**), suggesting that the dominant degradation stage in this system was the release of first bromine from TBBPA. Another main residual product

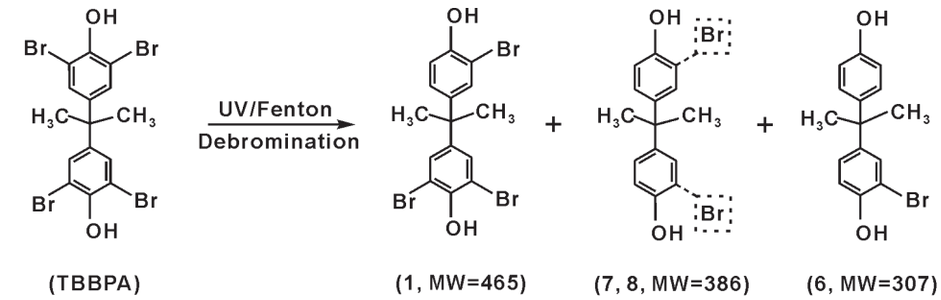

Scheme 1: Debromination processes

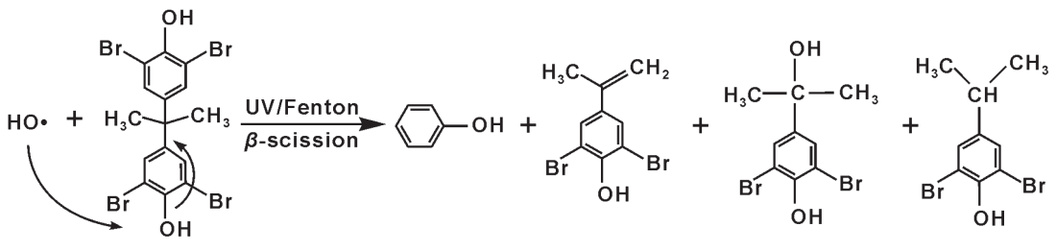

Scheme 2: Decomposition and transformation processes

Figure 10. Proposed reaction schemes for TBBPA degradation in UV/Fenton reaction catalyzed by $Fe_{2.04}Cr_{0.96}O_4$. (The uncertain substituent position of bromines was displayed in dotted boxes).

was identified as phenol (**2**), about 8.6%. The individual ratio of other six residual products was less than 2.0%. They were 4-isopropylene-2,6-debromophenol (**3**), 4-(2-hydroxyisopropyl)-2,6-dibromophenol (**4**), 4-isopropyl-2,6-dibromophenol (**5**), monobromobisphenol A (**6**) and two isomers of dibromobisphenol A (**7** and **8**).[25, 28, 47–49]

Due to the stronger catalytic activity of $Fe_{2.04}Cr_{0.96}O_4$, TBBPA in its system was almost completely degraded, and only six residual products were found after 240 min reaction. 63% of the products were identified as phenol (Products **2** in Fe_3O_4 containing system), and the relative percentage of Products **1** and **4**–**6** were 11.2%, 6.2%, 2.0% and 9.3%, respectively. Besides, Product **3** was not found, but one isomer of dibromobisphenol A (**7**) with percentage of 8.3% was detected. Therefore, both of the debromination and β-scission reaction were the dominant pathways for TBBPA degradation in UV/Fenton reaction catalyzed by $Fe_{2.04}Cr_{0.96}O_4$ (Fig. 10). Therefore, the $^{\bullet}$OH radicals may preferentially attack the C—Br bonds of TBBPA, and then β-cleavage the C—C bonds between benzene rings and isopropyl groups. It was worth mentioning that all these products in this system were not detected finally and TBBPA was mineralized through the heterogeneous UV/Fenton reaction catalyzed by $Fe_{2.04}Cr_{0.96}O_4$.

4. CONCLUSIONS

In the present study, the heterogeneous UV/Fenton degradation of TBBPA catalyzed by nanocrystalline magnetites Fe_3O_4 and $Fe_{2.04}Cr_{0.96}O_4$ was investigated. Neutral pH and UV radiation enhanced the TBBPA degradation. All the degradation processes at different initial pH were well fitted by the pseudo-first-order equation in kinetics. The chromium substitution obviously increased the BET surface area and superficial hydroxyl amount, and accelerated $^{\bullet}$OH radical generation, both of which improved the TBBPA degradation. In the UV/Fenton system catalyzed by $Fe_{2.04}Cr_{0.96}O_4$, the generated $^{\bullet}$OH radicals preferentially attacked the C—Br bonds of TBBPA and then β-cleavaged the C—C bonds between benzene rings and isopropyl groups. The above results are of high importance for well understanding the effect of Cr substitution on the UV/Fenton catalytic activity of magnetite, and prospecting the application of magnetite minerals for environmental purification.

Acknowledgments: This is contribution No. IS-1594 from GIGCAS. We would like to thank Shanghai Synchrotron Radiation Facility (SSRF) for providing us the beam time for the XAFS measurement. This work was financially supported by the National Natural Science Foundation of China (Grant Nos. 41172045 and 41103056) and Shanghai Tongji Gao Tingyao Environmental Science and Technology Development Foundation (STGEF).

References and Notes

1. S. H. Xu, D. L. Feng, W. Lu, S. J. Zhao, C. Y. Ma, D. D. Tan, and W. F. Shangguan, *Sci. Adv. Mater.* 5, 987 (**2013**).
2. Q. Y. Chen, X. Gu, Y. H. Wang, and D. W. Jing, *Sci. Adv. Mater.* 5, 1117 (**2013**).

3. L. P. Wang, S. K. Tang, and H. Zhou, *Sci. Adv. Mater*. 5, 822 **(2013)**.
4. L. Y. Chen and J. Zhang, *Sci. Adv. Mater*. 4, 859 **(2012)**.
5. C. M. Babu, B. Palanisamy, B. Sundaravel, M. Palanichamy, and V. Murugesan, *J. Nanosci. Nanotechnol.* 13, 2517 **(2013)**.
6. G. R. Chaudhary, P. Saharan, A. Kumar, S. K. Mehta, S. Mor, and A. Umar, *J. Nanosci. Nanotechnol.* 13, 3240 **(2013)**.
7. R. M. Lago, R. C. C. Costa, F. C. C. Moura, J. D. Ardisson, and J. D. Fabris, *Appl. Catal. B-Environ.* 83, 131 **(2008)**.
8. M. Usman, P. Faure, C. Ruby, and K. Hanna, *Chemosphere* 87, 234 **(2012)**.
9. S. P. Sun and A. T. Lemley, *J. Mol. Catal. A*: *Chem.* 349, 71 **(2011)**.
10. S. Anandan, G. J. Lee, S. H. Hsieh, M. Ashokkumar, and J. J. Wu, *Ind. Eng. Chem. Res*. 50, 7874 **(2011)**.
11. X. B. Luo, C. C. Wang, S. L. Luo, R. Z. Dong, X. M. Tu, and G. S. Zeng, *Chem. Eng. J*. 187, 45 **(2012)**.
12. X. L. Liang, Y. H. Zhong, S. Y. Zhu, J. X. Zhu, P. Yuan, H. P. He, and J. Zhang, *J. Hazard. Mater*. 181, 112 **(2010)**.
13. X. L. Liang, S. Y. Zhu, Y. H. Zhong, J. X. Zhu, P. Yuan, H. P. He, and J. Zhang, *Appl. Catal. B-Environ*. 97, 151 **(2010)**.
14. M. Hermanek, R. Zboril, N. Medrik, J. Pechousek, and C. Gregor, *J. Am. Chem. Soc*. 129, 10929 **(2007)**.
15. F. Magalhaes, M. C. Pereira, S. E. C. Botrel, J. D. Fabris, W. A. Macedo, R. Mendonca, R. M. Lago, and L. C. A. Oliveira, *Appl. Catal. A*: *Gen*. 332, 115 **(2007)**.
16. C. G. Ramankutty, S. Sugunan, and B. Thomas, *J. Mol. Catal. A-Chem*. 187, 105 **(2002)**.
17. L. C. A. Oliveira, J. D. Fabris, R. R. V. A. Rios, W. N. Mussel, and R. M. Lago, *Appl. Catal. A*: *Gen*. 259, 253 **(2004)**.
18. L. C. A. Oliveira, R. V. R. A. Rios, J. D. Fabris, V. Garg, K. Sapag, and R. M. Lago, *Carbon* 40, 2177 **(2002)**.
19. K. Sreekumar, T. Mathew, R. Rajgopal, R. Vetrivel, and B. S. Rao, *Catal. Lett*. 65, 99 **(2000)**.
20. R. C. C. Costa, M. de Fatima, F. Lelis, L. C. A. Oliveira, J. D. Fabris, J. D. Ardisson, R. R. V. A. Rios, C. N. Silva, and R. M. Lago, *Catal. Commun.* 4, 525 **(2003)**.
21. R. C. C. Costa, M. F. F. Lelis, L. C. A. Oliveira, J. D. Fabris, J. D. Ardisson, R. R. V. A. Rios, C. N. Silva, and R. M. Lago, *J. Hazard. Mater.* 129, 171 **(2006)**.
22. J. H. Deng, J. Y. Jiang, Y. Y. Zhang, X. P. Lin, C. M. Du, and Y. Xiong, *Appl. Catal. B*: *Environ*. 84, 468 **(2008)**.
23. X. L. Liang, Y. H. Zhong, H. P. He, P. Yuan, J. X. Zhu, S. Y. Zhu, and Z. Jiang, *Chem. Eng. J.* 191, 177 **(2012)**.
24. X. L. Liang, Y. H. Zhong, S. Y. Zhu, L. Y. Ma, P. Yuan, J. X. Zhu, H. P. He, and Z. Jiang, *J. Hazard. Mater*. 199, 247 **(2012)**.
25. Y. H. Zhong, X. L. Liang, Y. Zhong, J. X. Zhu, S. Y. Zhu, P. Yuan, H. P. He, and J. Zhang, *Water Res*. 46, 4633 **(2012)**.
26. S. Kitamura, N. Jinno, S. Ohta, H. Kuroki, and N. Fujimoto, *Biochem. Biophys. Res. Commun.* 293, 554 **(2002)**.
27. L. S. Birnbaum and D. F. Staskal, *Environ. Health Perspect.* 112, 9 **(2004)**.
28. K. D. Lin, W. P. Liu, and J. Gan, *Environ. Sci. Technol.* 43, 4480 **(2009)**.
29. S. Luo, S. G. Yang, C. Sun, and X. D. Wang, *Water Res.* 45, 1519 **(2011)**.
30. S. J. Yang, H. P. He, D. Q. Wu, D. Chen, X. L. Liang, Z. H. Qin, M. D. Fan, J. X. Zhu, and P. Yuan, *Appl. Catal. B*: *Environ.* 89, 527 **(2009)**.
31. W. G. Hu, Y. L. Su, D. J. Sun, and C. G. Zhang, *Langmuir*. 17, 1885 **(2001)**.
32. X. L. Liang, Y. H. Zhong, W. Tan, J. X. Zhu, P. Yuan, H. P. He, and Z. Jiang, *J. Therm. Anal. Calorim.* 111, 1317 **(2012)**.
33. M. L. Peterson, A. F. White, G. E. Brown, and G. A. Parks, *Environ. Sci. Technol*. 31, 1573 **(1997)**.
34. Y. Zhang, M. Yang, X. M. Dou, H. He, and D. S. Wang, *Environ. Sci. Technol*. 39, 7246 **(2005)**.
35. K. Nagaveni, G. Sivalingam, M. S. Hedge, and G. Madras, *Appl. Catal. B-Environ*. 48, 83 **(2004)**.
36. M. Sorescu, A. Grabias, D. Tarabasanu-Mihaila, and L. Diamandescu, *J. Appl. Phys*. 91, 8135 **(2002)**.
37. J. X. Chen and L. Z. Zhu, *J. Photochem. Photobiol. A*: *Chemistry* 188, 56 **(2007)**.
38. Y. P. Chen, D. N. Wang, Y. M. Yin, L. Y. Wang, X. F. Wang, and M. X. Xie, *J. Agr. Food Chem*. 60, 10472 **(2012)**.
39. Z. H. Sun, L. Mao, Q. M. Xian, Y. J. Yu, H. Li, and H. X. Yu, *J. Environ. Sci.-China* 20, 1075 **(2008)**.
40. J. Y. Feng, X. J. Hu, and P. L. Yue, *Water Res*. 40, 641 **(2006)**.
41. S. S. Chou, C. P. Huang, and Y. H. Huang, *Environ. Sci. Technol*. 35, 1247 **(2001)**.
42. J. Bandara, J. A. Mielczarski, and J. Kiwi, *Langmuir*. 15, 7670 **(1999)**.
43. V. Augugliaro, M. Pagliaro, V. Loddo, G. Palmisano, and L. Palmisano, Clean by light irradiation: practical applications of supported TiO_2, Royal Society of Chemistry, Cambridge **(2010)**, p. 19.
44. D. Nassoko, Y. F. Li, J. L. Li, X. Li, and Y. Yu, *Int. J. Photoenergy* 2012, 1 **(2012)**.
45. S. S. Lin and M. D. Gurol, *Environ. Sci. Technol*. 32, 1417 **(1998)**.
46. E. G. Garrido-Ramirez, B. K. G. Theng, and M. L. Mora, *Appl. Clay Sci.* 47, 182 **(2010)**.
47. J. Eriksson, S. Rahm, N. Green, A. Bergman, and E. Jakobsson, *Chemosphere* 54, 117 **(2004)**.
48. F. Barontini, V. Cozzani, K. Marsanich, V. Raffa, and L. Petarca, *J. Anal. Appl. Pyrol*. 72, 41 **(2004)**.
49. A. Hornung, A. I. Balabanovich, S. Donner, and H. Seifert, *J. Anal. Appl. Pyrolysis*. 70, 723 **(2003)**.

Received: 29 November 2012. Accepted: 24 December 2012.